

CLAMPING FORCE ESTIMATION BASED ON HYSTERESIS MODELING FOR ELECTRO-MECHANICAL BRAKES

Giseo Park¹⁾, Seibum Choi^{1)*} and Dongyoon Hyun²⁾

¹⁾Mechanical Engineering Department, KAIST, Daejeon 305-701, Korea

²⁾Chassis System Control Development Team, Hyundai Motor Company, 150 Hyundaiyeonguso-ro, Namyang-eup, Hwaseong-si, Gyeonggi 18280, Korea

(Received 21 April 2016; Revised 14 December 2016; Accepted 30 December 2016)

ABSTRACT–The Electro-Mechanical Brake (EMB) is anticipated by research communities and car manufacturers to be the future adopted brake system due to its advantages. However, to be competitively priced, the high cost load cell of EMB, which measures the clamping force to a disk, should be replaced by a clamping force estimation algorithm. For this purpose, a new clamping force estimator, compatible with readily available sensors, is proposed in this paper. This estimator determines the kissing point where the brake pads start to come into contact with the disk, and generates the characteristic curve of the polynomial function between the clamping force and the motor angle. Periodically updating the characteristic curve can enhance robustness to the pad’s changing thickness. Also, the model includes a description of the hysteresis of the clamping force in the overall algorithm, which prevents the estimation performance from decreasing in the transient state. The performance of the propose algorithm was validated by comparison with measured values on a developed EMB test bench.

KEY WORDS : Electro-Mechanical Brake (EMB), Clamping force, Kissing point, Hysteresis, Estimation

NOMENCLATURE

θ_s : electrical rotor angle, rad
 w_m, w_s : motor/synchronous angular velocity, rad/s
 i_d, i_q : motor current of d-axis/q-axis, A
 v_d, v_q : motor voltage of d-axis/q-axis, V
 L_d, L_q : self inductance of d-axis/q-axis, H
 R : stator resistance, Ω
 ψ_{af} : flux linkage, Wb
 n_p : number of pole pairs, -
 T_m : motor torque, Nm
 K_m : motor-torque constant, Nm/A
 θ_m : motor angle, rad
 p : pitch of ball screw, m
 GR : total gear ratio, -
 x_{screw} : displacement of ball screw, m
 k_{screw} : translating gain of ball screw, m
 k_{cl} : gearing gain, m
 F : clamping force, N
 η : efficiency of ball screw, -
 J_{tot} : total inertia, kg·m²
 T_L : load torque, Nm
 T_f : friction torque, Nm
 θ_0 : kissing point, rad
 $f_{cl}(\theta_m)$: characteristic curve, -

SUBSCRIPTS

for, back : forward/backward movement

1. INTRODUCTION

X-By-Wire (XBW) systems provide both convenience and high performance to drivers, and are expected to be common chassis systems in future vehicles. In particular, conventional hydraulic brake systems, which have complex hydraulic components, can be effectively replaced by a Brake-By-Wire (BBW) system, one of the XBW systems (Ki *et al.*, 2013). The structural differences between the hydraulic and BBW systems are shown in Figure 1. BBW system has many strengths, including fast response based on the use of electrical signals versus hydraulics, and by operating without the need for hydraulic components, makes better use of space. Furthermore, BBW system can be easily integrated with current advanced vehicle chassis control systems, such as Anti-lock Brake Systems (ABS) and Electronic Stability Control (ESC) systems. Due to increasing interest in BBW, the main actuator of BBW system, the Electro-Mechanical Brake (EMB), is now a subject of study among research communities and car manufacturers (Schwarz *et al.*, 1998; Line *et al.*, 2004; Hoseinnezhad *et al.*, 2008).

However, before production vehicles can be equipped with EMB, the high cost load cell, which is presently

*Corresponding author. e-mail: sbchoi@kaist.ac.kr

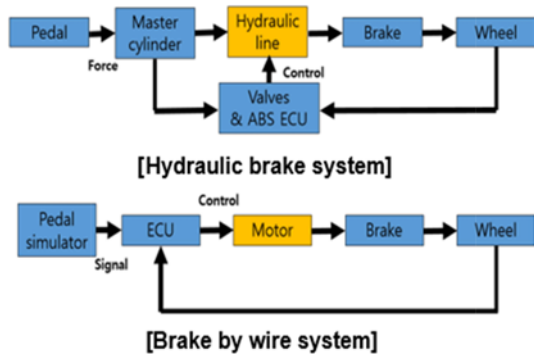


Figure 1. Diagrams of brake systems.

required for measuring the brake clamping force, has to be taken into account (Schwarz *et al.*, 1999; Saric *et al.*, 2008; Ki *et al.*, 2013). In addition, the load cell has other disadvantages, including difficulty of installation and low accuracy at high temperature. To solve these issues, algorithms for estimating the clamping force have been proposed in precious studies. A method for generating a characteristic curve of the clamping force versus the motor angle has been commonly utilized for this purpose (Schwarz *et al.*, 1999; Saric *et al.*, 2008; Ki *et al.*, 2013).

Actually, the values of clamping force at the same motor angle are not entirely consistent, and can be different depending on the direction of movement, i.e., forward and backward. To improve the estimation accuracy, a new algorithm is proposed in this paper, which handles the hysteresis effects of the clamping force. For this purpose, firstly, both the electrical and mechanical parts of EMB were mathematically expressed for modeling of EMB. On the basis of these models, a characteristic curve with the determined kissing point was generated. The estimated values of the clamping force considering the hysteresis effect were then compared with the actual values measured by a load cell. All experiments were implemented on a developed EMB test bench.

2. EMB MODELING

The overall structure of an EMB is shown in Figure 2 (Park *et al.*, 2016). A driver’s command is entered into a permanent magnet synchronous motor (PMSM). Then, the rotational motion of this PMSM is translated to reduction gears and one planetary gear set connected to PMSM in series. By passing through a ball screw, the rotational motion is converted into the linear motion of the piston. When the piston and the brake pads press the wheel disk, the caliper body simultaneously clamps the wheel disk from both sides. Generally, this caliper body accounts for a significant portion of the brake stiffness compliance (Schwarz *et al.*, 1999).

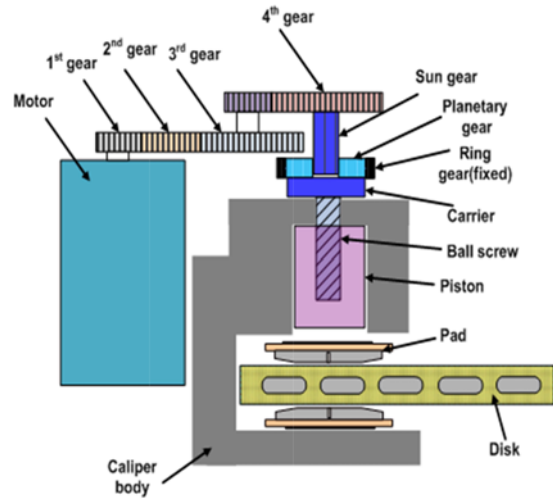


Figure 2. EMB structure.

2.1. Electrical and Mechanical Modeling

In the electrical modeling, PMSM is the appropriate actuator for EMB control based on its ability to control both motor velocity and motor current precisely (Zhong *et al.*, 1997; Prokop *et al.*, 2012). Three phase vectors with respect to a voltage or a current are transformed to rotor coordinates, the d-q axis. For the computation, the Clarke transform and Park transform are utilized in order (Pillay and Krishnan, 1989; Ki *et al.*, 2013). As a result, the voltage equations of PMSM are represented as follows (Zhong *et al.*, 1997; Prokop *et al.*, 2012; Park and Choi, 2013; Ki *et al.*, 2013):

$$v_d = Ri_d + L_d \frac{di_d}{dt} - w_s L_q i_q \tag{1}$$

$$v_q = Ri_q + L_q \frac{di_q}{dt} + w_s (L_d i_d + \psi_{ar}) \tag{2}$$

where

$$w_s = n_p w_m .$$

The motor torque of PMSM is derived as follows:

$$T_m = \frac{3}{2} n_p [\psi_{ar} i_q + (L_d - L_q) i_d i_q] . \tag{3}$$

To create the maximum motor torque, PMSM is controlled such that the motor current of the d-axis becomes zero (Zhong *et al.*, 1997; Prokop *et al.*, 2012; Park and Choi, 2013). Therefore, Equation (3) can be rewritten as the following simple formula.

$$T_m = \frac{3}{2} n_p \psi_{ar} i_q = K_m i_q \tag{4}$$

In the mechanical modeling, the displacement of the ball screw is expressed as a function which is linearly proportional to the motor angle (Jo *et al.*, 2010; Schwarz *et al.*, 1999).

$$x_{\text{screw}} = \frac{1}{GR_{\text{tot}}} \frac{p}{2\pi} \theta_m = k_{\text{screw}} \theta_m \quad (5)$$

From the linear motion, the load torque T_L , which is a function of the clamping force, is generated (Jo *et al.*, 2010; Schwarz *et al.*, 1999).

$$T_L = \frac{k_{\text{screw}}}{\eta} F_{\text{cl}} = k_{\text{cl}} F_{\text{cl}} \quad (6)$$

Lastly, the torque balance equation of EMB is derived as follows (Schwarz *et al.*, 1999; Saric *et al.*, 2008; Line *et al.*, 2008):

$$T_m = T_L + J_{\text{tot}} \frac{d^2 \theta_m}{dt^2} + T_f. \quad (7)$$

In an EMB system, T_f can be regarded as a kinetic coulomb friction model, whose sign is changed depending on the direction of movement, forward and backward (Saric *et al.*, 2008; Schwarz *et al.*, 1999; Olsson *et al.*, 1998).

2.2. Controller Design

As shown in Figure 3, the overall controller has a cascaded architecture. Every controller is a PI controller based on both proportional and integral feedback terms. For the stability of the overall controller, each feedback gain is determined by considering the pole placement (Ki *et al.*, 2013). Depending on the situation, one loop between the motor angle and clamping force controllers is selected as the outer control loop. To develop the clamping force estimator, the motor angle controller, where the measured values of the encorder are fed back, is selected. After this development, the load cell can be replaced by the estimator logics and then the clamping force controller can be operated while driving a car. However, in driving a car, the motor angle controller is operated whenever the motor angle has to return to zero (Ki *et al.*, 2013).

3. CLAMPING FORCE ESTIMATION

The main idea of clamping force estimation is fitting the characteristic curve of the clamping force, the second-order polynomial function (Schwarz *et al.*, 1999; Saric *et al.*, 2008; Ki *et al.*, 2013; Jo *et al.*, 2010; Line *et al.*, 2008). Since it is impractical to interrupt a driver's maneuvers while driving a car, it is recommended that the characteristic curve would be developed when starting the

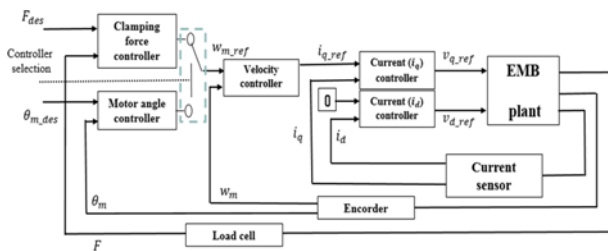


Figure 3. Block diagrams of EMB controller.

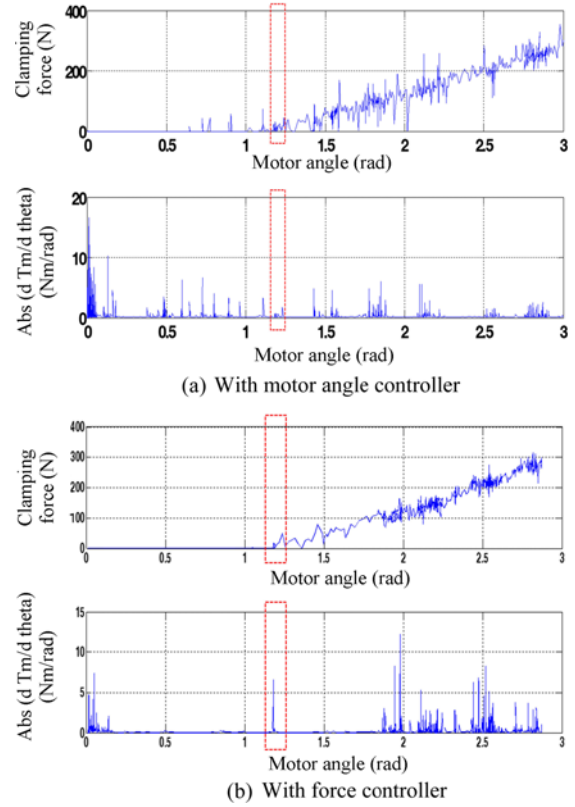


Figure 4. Previous algorithm for kissing point detection.

car. In particular, one cyclic brake command is automatically entered into the EMB ECU.

3.1. Kissing Point Detection

The kissing point, which is the motor angle where the pads start to come into contact with the disk, denotes the starting point of the characteristic curve. Therefore, the kissing point estimation affecting the performance of clamping force estimator has to be exactly estimated. Schwarz *et al.* (1999) proposed a kissing point detection method: the motor angle where the absolute value of the differential, $|dT_m/d\theta_m|$ becomes over threshold is regarded as the kissing point (Schwarz *et al.*, 1999; Jo *et al.*, 2010; Ki *et al.*, 2013).

Note that this method exploits the change of $|d\theta_m/dt|$; when the pads start to come into contact with the disk, the change of $|d\theta_m/dt|$ which affects the change of $|dT_m/d\theta_m|$ is not significant in the motor angle controller. As shown in Figure 4, it can be confirmed that the previous method with the clamping force controller detects the kissing point exactly, but on the contrary, the method with the motor angle controller cannot do it. As mentioned above, the motor angle controller is only used in the initialization of the estimation algorithm. Therefore, it is necessary to control the motor current directly to monitor the change of $|dT_m/d\theta_m|$. In this paper, a new kissing point detection algorithm with the motor angle controller is proposed.

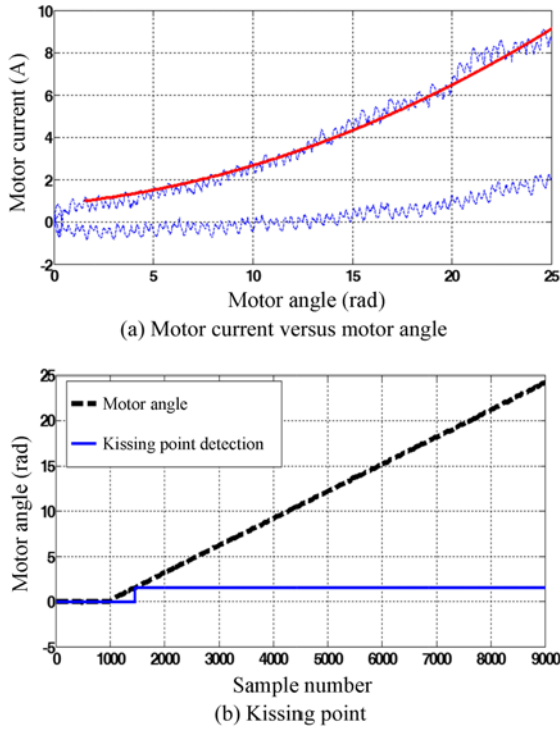


Figure 5. New algorithm for kissing point detection.

As shown in Figure 5 (a), the motor angle and motor current to which the signal filtering process is applied are measured during one cyclic brake command. Before the brake pads come into contact with the disk, the motor current is relatively small and steady.

Therefore, when the motor current becomes greater than the constant threshold i_0 , the motor angle at that time can be regarded as the kissing point. Since the measured data of motor current has noise and fluctuation, the second order fitted curve by a least square method is used for the kissing point detection. The curve is as shown in Figure 5 (a). Figure 5 (b) illustrates the correctly detected kissing point of the corresponding brake command in Figure 5 (a). If the pad thickness decreases due to pad wear, the kissing point will be changed (Saric *et al.*, 2009). Therefore, considering the change of pad thickness, the kissing point has to be estimated periodically.

3.2. Characteristic Curve

Considering the direction of the ball screw moving forward or backward and also the motor torque replaced by the motor current terms, Equation (7) is rewritten as Equations (8) and (9).

$$\text{Forward: } F_{cl} = \frac{1}{k_{cl}} \left(K_m i_{q-\text{for}} - J_{\text{tot}} \frac{d^2 \theta_{m-\text{for}}}{dt^2} + T_f \right) \quad (8)$$

$$\text{Back: } F_{cl} = \frac{1}{k_{cl}} \left(K_m i_{q-\text{back}} - J_{\text{tot}} \frac{d^2 \theta_{m-\text{back}}}{dt^2} - T_f \right) \quad (9)$$

To exploit the property of the coulomb friction torque T_f ,

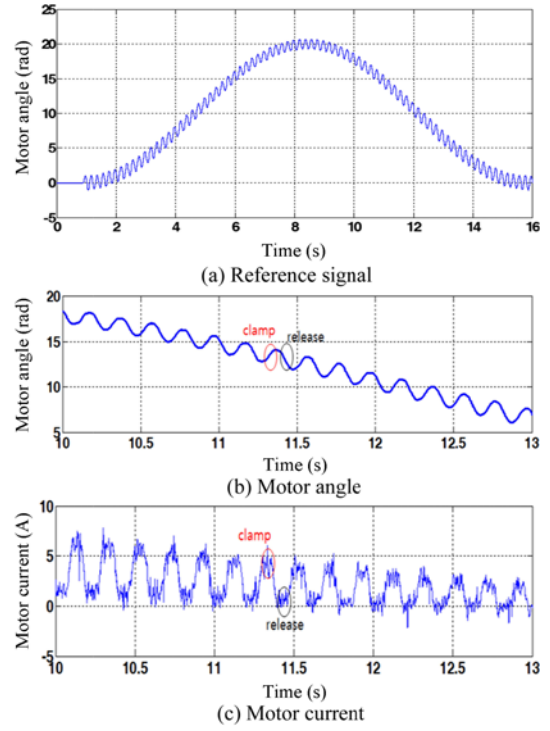


Figure 6. Reference signals.

a reference signal of the motor angle is introduced in Figure 6 (a). A sinusoidal wave with high frequency and low amplitude is superposed onto the smooth brake command. As shown in Figures 6 (b) and (c), the change of the motor current during the sinusoidal wave can be observed in detail. For the cases where $\theta_{\text{for}} = \theta_{\text{back}}$, the absolute value of the friction torque is assumed to be the same but with opposite signs because it has the same motor angle (Schwarz *et al.*, 1999; Karnopp, 1985). Hence, the friction term can be cancelled out. The estimated clamping force is represented as the following.

$$\hat{F}_{cl} = \frac{K_m}{2k_{cl}} (i_{q-\text{for}} + i_{q-\text{back}}) - \frac{J_{\text{tot}}}{2k_{cl}} \left(\frac{d^2 \theta_{m-\text{for}}}{dt^2} + \frac{d^2 \theta_{m-\text{back}}}{dt^2} \right) \quad (10)$$

From the measured values during forward movement, e.g. the range up to 8 seconds in Figure 6 (a), the

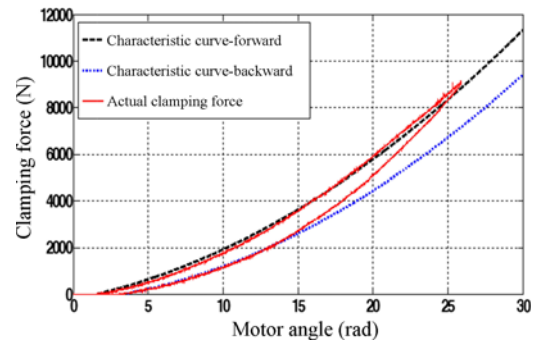


Figure 7. Characteristic curves and actual clamping force.

characteristic curve is derived as the following equation.

$$f_{cl-for}(\theta_m) = K_2(\theta_m - \hat{\theta}_{0-for})^2 + K_1(\theta_m - \hat{\theta}_{0-for}) \quad (11)$$

$\hat{\theta}_{0-for}$ is the detected kissing point. Also K_2 and K_1 are coefficients calculated by a least square method.

In a similar manner, from the measured values during backward movement, e.g. the range after 8 seconds in Figure 6 (b), the characteristic curve is derived as Equation (12).

$$f_{cl-back}(\theta_m) = K_3(\theta_m - \hat{\theta}_{0-back})^2 + K_4(\theta_m - \hat{\theta}_{0-back}) \quad (12)$$

$$\hat{\theta}_{0-back} = \hat{\theta}_{0-for} + \alpha \quad (13)$$

$\hat{\theta}_{0-back}$ is the shifted kissing point. The shifting factor α varies with the thickness of the brake pad. Figure 7 shows the characteristic curves in comparison with the actual clamping force versus the motor angle.

4. HYSTERESIS OF CLAMPING FORCE

In Figure 7, the characteristic curve during forward movement is very close to the actual value, but on the contrary, the characteristic curve during backward movement is different from the actual value during the transient state near the switching point (θ_R, F_R) where the direction of movement is changed from forward to backward (Ki *et al.*, 2013). Thus, when the sign of angular velocity w_m is changed, the motor angle θ_m at that time is regarded as θ_R . Also, $F_R = f(\theta_R)$ is obtained from the estimated characteristic curve.

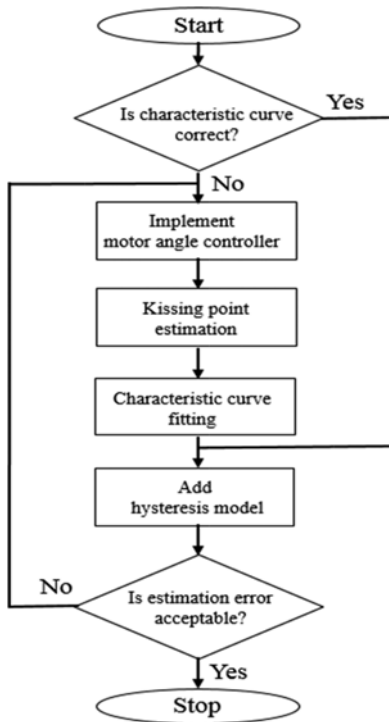


Figure 8. Development flowchart for estimator.

The difference, i.e., the hysteresis of the clamping force, occurs consistently even during the change of direction from backward to forward. To enhance the estimation performance, these hysteresis effects are mathematically modeled. The development flowchart for the estimator including the hysteresis model is illustrated in Figure 8.

4.1. Mechanism of Hysteresis

One of the reasons hysteresis occurs in the transient state is the actuation phase lag due to internal friction. The motor, reduction gears, ball screw, and the piston are not one rigid body but are components of EMB connected to each other. After a driver's command for the direction change is entered into the motor, the direction of the friction torque is sequentially changed in the order of the motor, reduction gears, ball screw, and the piston. The clamping force in the transient state is affected by this sequential change of the friction. Also, both gear backlash (Ki *et al.*, 2013) and the elastic hysteresis of the brake pads can cause hysteresis of the clamping force. Figure 9 shows the changes of direction at some random switching points and the resulting hysteresis effects. Under the condition that the kissing point stays equal, it is confirmed that the clamping force converges to the characteristic curve $f_{cl-back}(\theta_m)$ regardless of the switching points.

4.2. Modeling of Hysteresis

To develop the hysteresis model of clamping force, the convergence property is exploited. During forward movement, the differential equation of the clamping force with respect to the motor angle is derived as follows:

$$\frac{d\hat{F}_{cl}}{d\theta_m} = -k_1(\hat{F}_{cl} - f_{cl-for}(\theta_m)) \quad (14)$$

$$\frac{d\hat{F}_{cl}}{(\hat{F}_{cl} - f_{cl-for}(\theta_m))} = -k_1 d\theta_m$$

k_1 is the tuning gain, $f_{cl-for}(\theta_m)$ the characteristic curve during forward movement, and (θ_R, F_R) the switching

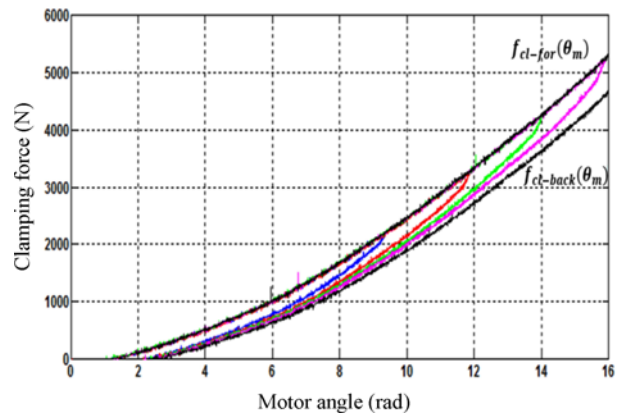
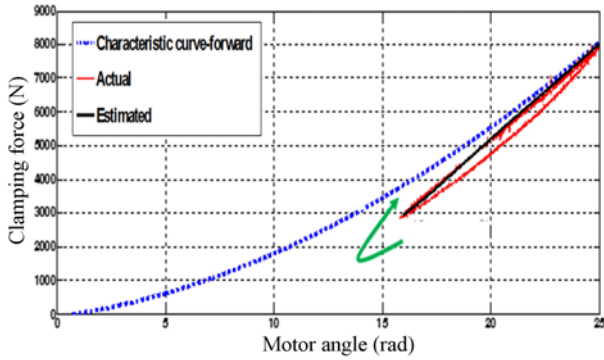
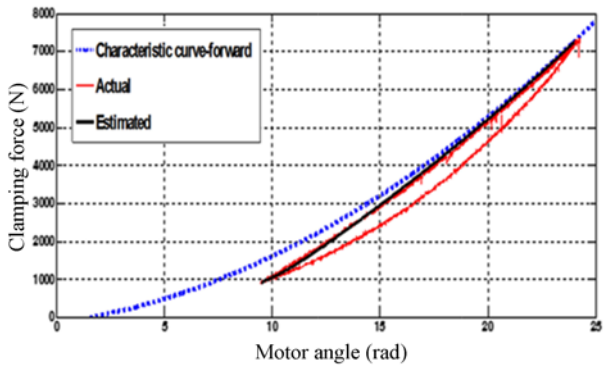


Figure 9. Random switching points.



(a) Switching point of 16 rad



(b) Switching point of 9 rad

Figure 10. Modeling of hysteresis in forward movement.

point from backward to forward. By integrating Equation (14), \hat{F}_{cl} is derived as follows:

$$\int_{F_R}^{\hat{F}_{cl}} \frac{d\hat{F}_{cl}}{(\hat{F}_{cl} - f_{cl-for}(\theta_m))} = \int_{\theta_R}^{\theta_m} -k_1 d\theta_m \quad (15)$$

$$\ln \frac{\hat{F}_{cl} - f_{cl-for}(\theta_m)}{F_R - f_{cl-for}(\theta_m)} = k_1(\theta_m - \theta_R)$$

$$\hat{F}_{cl} = (F_R - f_{cl-for}(\theta_m))e^{-k_1(\theta_m - \theta_R)} + f_{cl-for}(\theta_m) \quad (16)$$

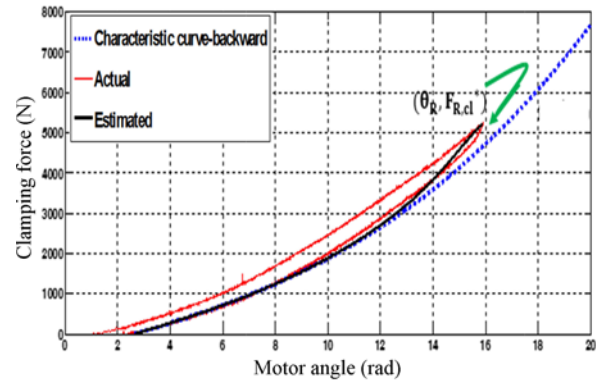
When the direction is changed from backward to forward at the switching points 16 rad and 9 rad, the estimated values \hat{F}_{cl} are very close to the actual ones measured by a load cell (see Figure 10).

By simply varying the parameter k_1 within the range from 0.2 to 0.5, the transient characteristics can be well represented. Although k_1 varies with the pad thickness, it can be treated as a constant value during each brake operation since the change of pad thickness is very slow.

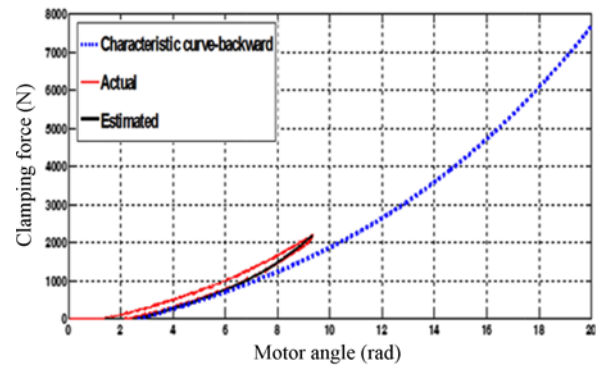
In the same way, the differential equation of the clamping force during the backward movement is derived as follows:

$$\frac{d\hat{F}_{cl}}{d\theta_m} = k_2(\hat{F}_{cl} - f_{cl-back}(\theta_m)) \quad (17)$$

$$\frac{d\hat{F}_{cl}}{(\hat{F}_{cl} - f_{cl-back}(\theta_m))} = k_2 d\theta_m$$



(a) Switching point of 16 rad



(b) Switching point of 9 rad

Figure 11. Modeling of hysteresis in backward movement.

where the gain k_2 takes a role of k_1 in Equation (14).

$$\int_{F_R}^{\hat{F}_{cl}} \frac{d\hat{F}_{cl}}{(\hat{F}_{cl} - f_{cl-back}(\theta_m))} = \int_{\theta_R}^{\theta_m} -k_2 d\theta_m \quad (18)$$

$$\ln \frac{\hat{F}_{cl} - f_{cl-back}(\theta_m)}{F_R - f_{cl-back}(\theta_m)} = -k_2(\theta_m - \theta_R)$$

Like Equation (16), \hat{F}_{cl} is derived as follows:

$$\hat{F}_{cl} = (F_R - f_{cl-back}(\theta_m))e^{-k_2(\theta_m - \theta_R)} + f_{cl-back}(\theta_m) \quad (19)$$

As shown in Figure 11, the high accuracy of \hat{F}_{cl} can be confirmed.

5. EXPERIMENTAL RESULTS

All the experiments in this study were implemented on a developed EMB test bench (see Figure 12). To take the effect of pad thickness into account, brake pads of 3 mm, 6 mm, and 13 mm, shown in Figure 13, were used. In the controller area network (CAN), both the driver's command and the measured data are communicated through the control desk in the host PC and Micro-AutoBox where the proposed clamping force estimator was built. To develop the estimator, the actual parameters of EMB in Table 1 were utilized. The feedback cascaded controller was downloaded onto EMB ECU through the USB Multilink.

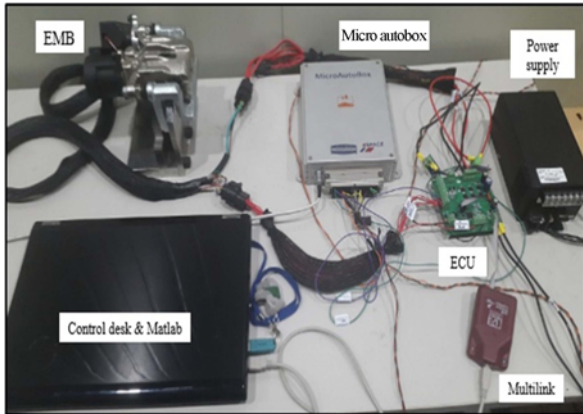


Figure 12. EMB test bench.



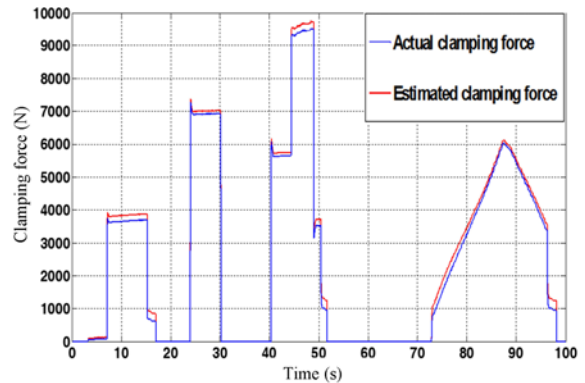
Figure 13. Brake pads.

Table 1. Parameters of EMB.

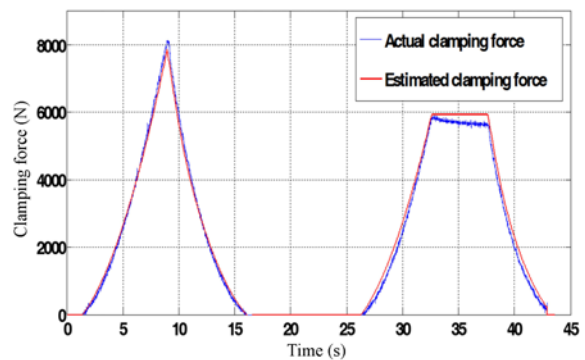
Parameter	Value
Motor resistance R	0.137 mΩ
Motor inductance L_d, L_q	93.5 μH
Motor torque constant K_m	0.047 Nm/A
Number of pole pairs n_p	3
Flux linkage ψ_{af}	0.00402 Wb
Total inertia moment J_{tot}	3.184×10^{-5} kg·m ²
Total gear ratio GR	39 : 1
Pitch of ball screw p	5 mm
Efficiency of ball screw η	68 %

Every process in the experiment can be monitored at a 1 ms sampling rate. To attenuate the high frequency noise of the measured values, a low pass filter with a fairly high bandwidth was applied to the actual values. The clamping force estimation results with the full pad thickness of 13 mm are shown in Figure 14.

In particular, due to the proposed hysteresis model, the estimation errors are very small in the transient states near some switching points. The Root Mean Square (RMS) error of 0.2 kN is smaller than the appraisal standard in this study, which is 0.4 kN (Chang *et al.*, 1993; Rajamani, 2006). Also, for the worn out pad thicknesses, 3 mm and 6 mm, the estimated clamping force is very close to the



(a) Result 1



(b) Result 2

Figure 14. Estimation results with pad thickness of 13 mm.

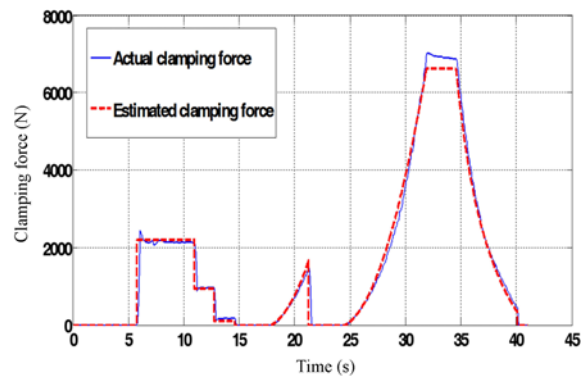


Figure 15. Estimation results with pad thickness of 6 mm.

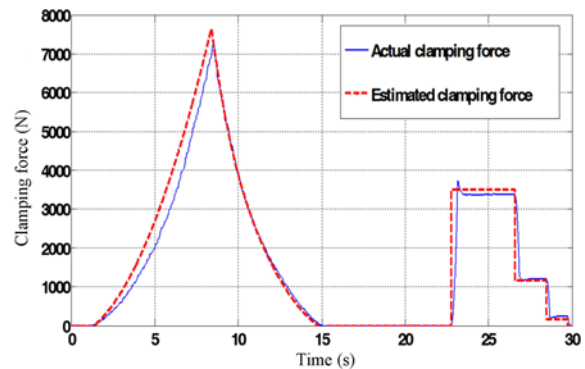


Figure 16. Estimation results with pad thickness of 3 mm.

actual one. RMS errors of 0.23 kN and 0.3 kN were recorded, respectively, which satisfy the goal of the estimation performance again.

6. CONCLUSION

In this paper, an EMB clamping force estimator which is compatible with readily available sensors was proposed. When the motor angle controller operates, characteristic curves for forward and backward movement are respectively generated by a least square method. By employing the kissing point detection algorithm, these characteristic curves can be made to be very similar to the actual clamping force measured by the load cell. The major contribution of this paper is the introduction of a model to deal with the hysteresis of the clamping force, which is mainly caused by the phase lag effect and the elastic characteristic of the brake pad. This hysteresis model ensures that the accuracy of the estimated clamping force can be equally well maintained even during the transient when changes of direction occur, between forward and backward.

In conclusion, the proposed estimation algorithm distinguishes itself from previous algorithms by the following features:

- (1) The kissing point, which affects the performance of the clamping force estimator, is determined by a practical and simple method;
- (2) Due to the periodical update of the characteristic curves, the proposed algorithm guarantees robust to the changes in pad thickness;
- (3) A novel method for intuitively describing the hysteresis of EMB clamping force is introduced.

It is anticipated that these results can be easily applied to current EMB hardware and contribute to the development of an outstanding BBW system.

ACKNOWLEDGEMENT—This work was supported by the National Research Foundation of Korea (NRF) grant funded by the Korea government (MSIP) (No. 2010-0028680) and the BK21 plus program through the NRF funded by the Ministry of Education Korea. This research was supported by the MSIP (Ministry of Science, ICT and Future Planning), Korea, under the C-ITRC (Convergence Information Technology Research Center) (ITTP-2016-H8601-16-1005) supervised by the ITTP (Institute for Information & communications Technology Promotion).

REFERENCES

- Chang, K., Hedrick, J., Zhang, W., Varaiya, P., Tomizuka, M. and Shladover, S. (1993). Automated highway system experiments in the PATH program. *J. Intelligent Transportation Systems* **1**, 1, 63–87.
- Hoseinnezhad, R., Bab-Hadiashar, A. and Rocco, T. (2008). Real-time clamp force measurement in electromechanical brake calipers. *IEEE Trans. Vehicular Technology* **57**, 2, 770–777.
- Jo, C., Hwang, S. and Kim, H. (2010). Clamping-force control for electromechanical brake. *IEEE Trans. Vehicular Technology* **59**, 7, 3205–3212.
- Karnopp, D. (1985). Computer Simulation of stick-slip friction in mechanical dynamic systems. *J. Dynamic Systems, Measurement, and Control* **107**, 1, 100–103.
- Ki, Y., Lee, K., Cheon, J. and Ahn, H. (2013). Design and implementation of a new clamping force estimator in electro-mechanical brake systems. *Int. J. Automotive Technology* **14**, 5, 739–745.
- Line, C., Manzie, C. and Good, M. (2004). Control of an electromechanical brake for automotive brake-by-wire systems with adapted motion control architecture. *SAE Paper No. 2004-01-2050*.
- Line, C., Manzie, C. and Good, M. (2008). Electromechanical brake modeling and control: From PI to MPC. *IEEE Trans. Control Systems Technology* **16**, 3, 446–457.
- Olsson, H., Astrom, K., Wit, C., Gafvert, M. and Lischinsky, P. (1998). Friction models and friction compensation. *European J. Control* **4**, 3, 176–195.
- Park, G., Hyun, D. and Choi, S. B. (2016). Development of clamping force estimation algorithm and clamp-force sensor calibration on electromechanical brake systems. *Trans. Korean Society of Automotive Engineers* **24**, 3, 365–371.
- Park, H. and Choi, S. B. (2013). The development of a sensorless control method for a self-energizing brake system using noncircular gears. *IEEE Trans. Control Systems Technology* **21**, 4, 1328–1339.
- Pillay, P. and Krishnan, R. (1989). Modeling, simulation, and analysis of permanent-magnet motor drives, Part I: The permanent-magnet synchronous motor drive. *IEEE Trans. Industry Applications* **25**, 2, 265–273.
- Prokop, L., Stulrajter, M. and Radhostem, R. (2012). 3-phase PMSM Vector Control Using the PXS20 and Tower System. Freescale Semiconductor Application Note, AN4537.
- Rajamani, R. (2006). *Vehicle Dynamics and Control*. Springer-Verlag, New York, USA.
- Saric, S., Bab-Hadiashar, A. and Hoseinnezhad, R. (2008). Clamp-force estimation for a brake-by-wire system: A sensor-fusion approach. *IEEE Trans. Vehicular Technology* **57**, 2, 778–786.
- Saric, S., Bab-Hadiashar, A. and Walt, J. (2009). Estimating clamp force for brake-by-wire systems: Thermal considerations. *Mechatronics* **19**, 6, 886–895.
- Schwarz, R., Isermann, R., Bhm, J., Nell, J. and Rieth, P. (1999). Clamping force estimation for a brake-by-wire actuator. *SAE Paper No. 1999-01-0482*.
- Schwarz, R., Isermann, R., Bohm, J., Nell, J. and Rieth, P. (1998). Modeling and control of an electromechanical disk brake. *SAE Paper No. 980600*.
- Zhong, L., Rahman, M., Hu, W. and Lim, K. (1997). Analysis of direct torque control in permanent magnet synchronous motor drives. *IEEE Trans. Power Electronics* **12**, 3, 528–536.